Soft Matter

RSC Publishing

PAPER

View Article Online
View Journal | View Issue

Published on 11 January 2013. Downloaded by The University of Melbourne Libraries on 16/07/2013 07:09:19.

Cite this: *Soft Matter*, 2013, **9**, 2426

Non-linear and cyclical collisions between drops and bubbles: using AFM to understand droplet interactions in micro-scale flows†

Rico F. Tabor,*[ab] Chu Wu,[bc] Franz Grieser,[bd] Derek Y. C. Chan[bce] and Raymond R. Dagastine*[bfg]

Understanding the mechanics and outcome of droplet and bubble collisions is central to a range of processes from emulsion stability to mineral flotation. The atomic force microscope has been shown to be sensitive and accurate in measuring the forces during such interactions; in combination with a suitable model framework, a powerful tool is obtained for understanding surface forces and droplet stability in dynamic systems. Here we demonstrate for the first time that this process is not limited to linear motion, and that accelerating, decelerating and cyclical droplet velocities can be used to explore the collisions between droplets and bubbles in ways that much more closely mimic real systems. In particular, the motion of droplets experiencing oscillating pumping pressures is explored, providing insight into fluid handling for microfluidics. By modelling a range of processes in which drops collide and deform, and sometimes coalesce, the validity of the theoretical model – which accounts for deformation, surface forces and dynamic lubrication – is demonstrated. Further, it is shown how this model can be used as a predictive tool to determine whether a given droplet collision will be stable or coalescent.

Received 25th October 2012
Accepted 3rd January 2013

DOI: 10.1039/c2sm27463a

www.rsc.org/softmatter

Introduction

The interaction between pairs of small droplets and bubbles underpins processes from emulsion formulation in foods and paints to digital microfluidics. In all cases, the same group of parameters control the outcome of such interactions – surface forces, hydrodynamics and deformation of the interfaces involved. In formulations such as emulsions and foams, bubbles and droplets are in continual motion, from natural Brownian dynamics and buoyancy or driven by the shear forces encountered in transport and processing. Thus an understanding of the mechanics of such interactions between small, deformable bodies over a range of velocity profiles is valuable.

Of particular interest is the miniaturisation of fluid flows in microfluidic (and now nanofluidic) devices, which has resulted in a rapidly growing field in which droplets and bubbles continually interact with one another.[1,2] The motivation for such miniaturisation is the potential for high throughput synthesis, screening and reactions, particularly desirable for example in biomedical systems[3] and drug discovery.[4] In order to increase the efficiency and throughput of devices with two-phase flows, increased dispersed phase volume fractions mean that bubbles and drops come into closer contact and thus an understanding of the conditions experienced by droplets and bubbles colliding is important. In particular, the final step in true process miniaturisation is to provide on-chip pumping with recent developments in peristaltic,[5] diaphragm-type[6] and passive pumping methods. In the case of either on- or off-chip pumping,[7] the characteristic fluid velocities provided by the pump drive result in different pressure fields, and hence different flow characteristics of drops. Increased droplet and bubble volume fractions make an understanding of this even more important.[8] When droplets interact either intentionally, through channel design or otherwise, their propensity to coalesce is controlled by the velocity profile of the collision, the surface forces between the drops and their ability to deform.[9]

[a]*School of Chemistry, Monash Univeristy, Clayton 3800, Australia. E-mail: rico.tabor@monash.edu; Fax: +61 3 9905 4597; Tel: +61 3 9905 4558*

[b]*Particulate Fluids Processing Centre, University of Melbourne, Parkville 3010, Australia*

[c]*Department of Mathematics and Statistics, University of Melbourne, Parkville 3010, Australia*

[d]*School of Chemistry, University of Melbourne, Parkville 3010, Australia*

[e]*School of Life and Social Sciences, Swinburne Univeristy of Technology, Hawthorn 3122, Australia*

[f]*Department of Chemical and Biomolecular Engineering, University of Melbourne, Parkville 3010, Australia. E-mail: rrd@unimelb.edu.au; Fax: +61 3 8344 4153; Tel: +61 3 8344 4704*

[g]*Melbourne Centre for Nanofabrication, 151 Wellington Road, Clayton 3168, Australia*

† Electronic supplementary information (ESI) available: Video files visualising the evolution of modelled force and film profiles for sinusoidal and accelerating drive functions. See DOI: 10.1039/c2sm27463a

This journal is © The Royal Society of Chemistry 2013

Published on 11 January 2013. Downloaded by The University of Melbourne Libraries on 16/07/2013 07:09:19.

The atomic force microscope (AFM) has been demonstrated to be a powerful and versatile tool for analysing the interactions between droplets and bubbles on the micron scale.[10] In particular, the AFM can directly control trajectories of colliding drops/bubbles to explore a range of interaction speeds and forces.[11] Such AFM experiments are clearly limited to interactions between pairs of drops, and any information on larger-scale systems or multi-body interactions must be inferred. However, by directly probing pair-wise droplet interactions, it is possible to determine the forces that the droplets experience during collision, and whether such collisions result in coalescence.[12,13] In doing so, a great deal has been learnt about surface and colloidal forces, hydrodynamics and the interplay with interfacial deformation.

Crucial to interpreting experimental measurements of such interactions is the theoretical model that has been developed to understand these systems.[14–16] Droplets or bubbles colliding with one another present a complex system where local deformation, their internal Laplace pressure, the hydrodynamic forces exerted by the fluid between them and the disjoining pressure (from surface or colloidal forces) must be accounted for to obtain a full description of the interaction. However, in doing so, a great deal of information can be obtained, including the shape of the fluid–fluid interfaces during the interaction, providing insight into the conditions and mechanistic requirements for coalescence or stability.[12,17]

Thus far, AFM studies of the dynamic interactions between pairs of bubbles and droplets have been restricted to linear velocity drives,[13,18–20] whereby bodies are moved together and separated at constant speed. This has been primarily due to experimental constraints related to the control and capabilities of AFM instrumentation, and the lack of a suitably robust modeling framework to analyse more complex data. Despite these limitations, significant insight into a range of physical phenomena has been gained. In the majority of real systems however, this is not a true depiction of what occurs. For example, two droplets driven toward one another by Brownian motion will slow as the separation between them decreases sufficiently for fluid resistance in the film to become important; this resistance also tends to cause drop deformation in the form of flattening or dimpling of the droplet interfaces. A similar effect is seen for a drop or bubble approaching a solid surface when driven[21] or rising due to buoyancy.[22] In driven flows, such as those encountered in microfluidic channels, even more elaborate droplet behaviour is seen, including the recent observation that droplets accelerating *away* from one another tend to coalesce.[23,24]

Here, we use the AFM to investigate controlled collisions between pairs of bubbles and droplets, 50–150 μm in diameter, driven with accelerating and decelerating droplet velocities, characteristic of fluid pumping flows.[25,26] A theoretical model is applied to understand the relationship between the way the drops are driven together and the outcome of such interactions. Using this construction, we deal with axisymmetric interactions only; the considerably more complex theoretical modelling needed to analyse oblique collisions is beyond the scope of the current study. We determine the conditions required for coalescence for several simple systems, and suggest additional new ways in which AFM can act as a powerful analytical tool for characterising behaviour in micro-scale fluid flows. It is seen that in addition to understanding the mechanics of droplet interaction, the AFM can provide information on the subtle interplay between surface forces, deformation and flow in droplet systems, giving both analytical and predictive insight for droplet dynamics, thus creating a 'map' of stability to guide liquid handling.

Experimental

Materials

Perfluorooctane (PFO, 99%) was obtained from Sigma, and purified by column chromatography over silica (Florisil, Sigma) before use. Deionised water was from a Millipore Milli-Q system, with a minimum resistivity of 18.4 MΩ cm. Sodium hydroxide and nitric acid solutions (both obtained from Lab-Supply and used as received) were used for pH adjustment. To generate bubbles, solutions were prepared from deionised water and adjusted to the required pH, and then used directly without additional sparging or gasification.

Methods

Rectangular silicon AFM cantilevers (450 × 50 × 2 μm) were custom made, with a circular gold pattern (diameter 45 μm, thickness ≈ 20 nm) added ≈5 μm from the end.[12] This gold region was rendered hydrophobic by adsorption of decanethiol in ethanol (1 mM) for 2 hours. Cantilever spring constants, K, were determined by the method of Hutter and Bechhoeffer,[27] and were in the range 0.1–0.2 N m^{-1}. The AFM measurements were performed on an Asylum MFP-3D AFM driven by an ARC1 controller. To effect motion in the Z (normal) direction, a voltage is applied to a piezoelectric stack, resulting in a motion, which is broadly proportional to the applied voltage. However, the AFM is equipped with a linear variable differential transformer (LVDT) sensor in the Z-movement direction to allow direct detection of cantilever Z-position during force measurements so that deviations in the response of the piezo stack with applied voltage can be quantified. Non-linear drive functions were created using simple piece-wise equations to obtain a displacement *vs.* time function, which was used as an input for the Asylum Research 'Force Maveric' function. This subroutine, implemented within the Igor Pro software environment that controls the MFP-3D back-converts the desired displacement *vs.* time function to a voltage *vs.* time input that is then applied to the piezo, resulting in the desired displacement as a function of time.

Bubbles were generated ultrasonically (Undatim Ultrasonics D-reactor), at a frequency of 515 kHz, and power of 25 W.[28] The substrates used for bubble generation were glass Petri dishes which had been cleaned and then partially hydrophobised through a silano-ether coupling reaction in absolute ethanol for 2 hours.[29] This was found to generate a surface of intermediate hydrophobicity (water contact angle ≈ 60°) suitable for immobilising bubbles but still allows them to be readily picked

Published on 11 January 2013. Downloaded by The University of Melbourne Libraries on 16/07/2013 07:09:19.

up and transferred to hydrophobic patch on the cantilever. For measurements involving PFO, droplets of the oil were generated by using a 100 μL syringe to disperse a few μL of the oil under water in a 6 cm Petri dish.[30] Bubbles and droplets used in these experiments were in the diameter range 80–140 μm.

In order to perform a measurement between two drops (or bubbles), a drop (or bubble) was picked up on a cantilever using the micro-positioning stage of the AFM, so that it formed a three-phase contact with the hydrophobised gold patch on the cantilever, defining its contact area precisely. This drop (or bubble) was then positioned over a similarly sized drop (or bubble) on the substrate, and the piezo drive of the AFM was used to perform interaction measurements in the Z direction only (normal to the substrate). The deflection of the cantilever was measured by the reflection of a laser beam from the back of the cantilever onto a split photo-diode, using the optical lever technique, and this deflection was converted to force using the cantilever spring constant and Hooke's law. An initial separation of approximately 2 μm was achieved by using a standard 'triggered' force curve (where the piezo is driven at constant velocity toward the surface until a certain deflection of the cantilever is reached (indicating close approach of the drops), after which point it retracts the required distance). By comparing the model prediction to the force curve generated, it is possible to obtain drop (or bubble) profiles in the interaction zone (thin film region) between drops (or bubbles) as a function of time, and hence calculate their separation and the geometry of the liquid film between them. Experiments were arranged and followed with high-magnification optical microscopy from below (Nikon TE2000). This allowed measurement of bubble and radii to be made to within ±2 μm, and also facilitated precise alignment to ensure axisymmetry during interactions. The process of arranging and performing AFM measurements between pairs of droplets and bubbles is explain in detail in ref. 10.

Theory

The model used to predict the behaviour of drops and bubbles is based on the Stokes–Reynolds–Young–Laplace model for analysis of AFM experiments.[15–17] This framework accounts for local deformation of interacting drop, the disjoining pressure in the liquid film of thickness $D(r,t)$ that separates them arising from surface or colloidal forces, the Laplace pressure inside the drops and dynamic drainage in the liquid film between them (see Fig. 1). The Young–Laplace equation is used to describe the deformation of drops/bubbles due to disjoining pressure, $\Pi(D)$ and hydrodynamic pressure, $p(r,t)$:

$$\frac{\sigma}{2r}\frac{\partial}{\partial r}\left(r\frac{\partial D}{\partial r}\right)=\frac{2\sigma}{R}-p-\Pi \qquad (1)$$

where σ is the interfacial tension, r is the radial coordinate and R is the harmonic mean of the two drop/bubble radii R_1 and R_2, calculated as $R^{-1}=(R_1{}^{-1}+R_2{}^{-1})/2$. By applying Reynolds lubrication theory in the Stokes flow regime, where the intervening liquid has viscosity μ, and assuming an immobile boundary condition at the drop/bubble interfaces (discussed later), the film thickness and hydrodynamic pressure are related as:

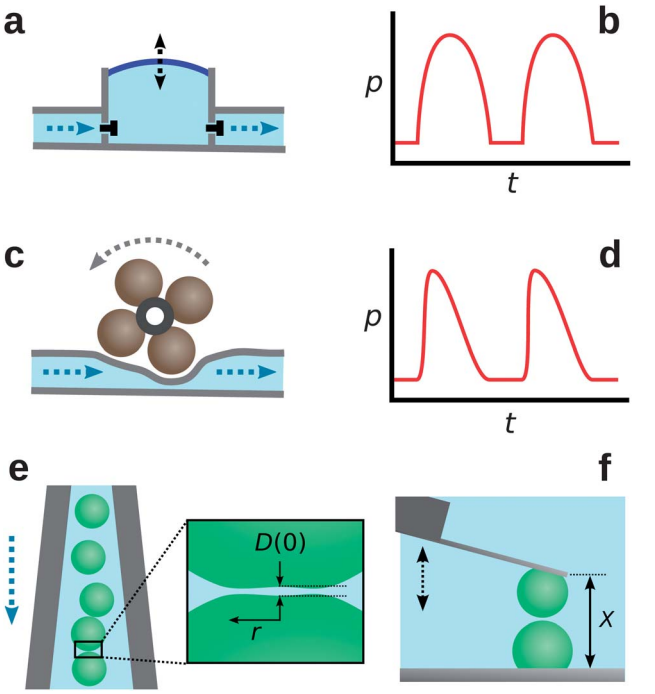

Fig. 1 Schematic diagrams showing (a) a simple diaphragm pump; (b) the characteristic pressure *vs.* time characteristics of a diaphragm pump; (c) a peristaltic pump; (d) the characteristic pressure *vs.* time characteristics of a peristaltic pump; (e) droplets in a microfluidic channel where the geometry causes their average separation to decrease. The zoomed region shows the film formed between two droplets at close approach. The central film thickness, $D(0)$ and radial coordinate r are labelled; (f) the AFM setup used, with a drop captured on the cantilever and one immobilised on a solid surface. The control parameter in AFM measurements is ΔX, the change in separation, X, between the end of the cantilever and the substrate.

$$\frac{\partial D}{\partial t}=\frac{1}{12\mu r}\frac{\partial}{\partial r}\left(rD^3\frac{\partial p}{\partial r}\right) \qquad (2)$$

This approach to calculating the dynamic force of interaction between deformable drops and bubbles has been described and reviewed in detail recently,[15,16] and so is not reproduced in full here.

Results and discussion

Collisions between droplets and bubbles can occur due to Brownian motion or driven fluid flows, such as those generated in shearing bulk samples or pumping in fluidic devices. Here, we concentrate on the latter, although it is important to note that the same principles of using accelerating and decelerating drives could equally be applied to understand the interactions of 'free' drops and bubbles that interact *via* natural Brownian dynamics and buoyancy.

The nature of collisions that can occur between droplets in microfluidic devices depends on the way in which the fluid flows are driven. Channel widths and geometries, pumping methods and pressures and fluid properties all have an important role in the velocity with which droplets will interact. Specifically, it has been seen that certain channel geometries

 This journal is © The Royal Society of Chemistry 2013

Published on 11 January 2013. Downloaded by The University of Melbourne Libraries on 16/07/2013 07:09:19.

appear to favour coalescence in metastable systems;[23,24] although deformation of the droplets by the channel can be the stimulus for such events, the interaction between drops themselves is still controlled by the behaviour of the thin liquid film between them. In this study, we focus on producing and analysing simple oscillatory drive functions to demonstrate the capability of the AFM as a tool for analysing collisions between droplets in actively pumped flows. Due to the different mechanical drive mechanisms of various types of pumping, they induce different characteristic outlet flow velocity profiles as illustrated schematically in Fig. 1.

Sinusoidal drive

To demonstrate the details and effectiveness of the approach, the first drive function chosen was a simple sinusoidal variation of displacement with time, shown in Fig. 2a. A bubble (radius 60 μm) is captured on the cantilever, and brought directly over a bubble (radius 45 μm) on the substrate. At the beginning of the measurement, the bubbles are approximately 2 μm apart (this distance having been obtained as described in the methods section) and are moved together and apart with an increasing amplitude, until coalescence occurs. That is, the bubbles are pushed slightly closer together on each successive 'cycle' until coalescence is observed. The piezo drive which actuates the movement in the *Z*-axis direction does not respond linearly with applied voltage and therefore it is crucial that the actual displacement is measured; on the instrument used in these experiments, this was achieved by means of a linear variable differential transformer (LVDT) sensor.‡ In Fig. 2b, the symbols are experimental AFM data of the force as measured by the AFM cantilever against time, and the solid lines are predictions using the theoretical model. The point at which the experimental bubbles coalesced is shown with a vertical dashed line.

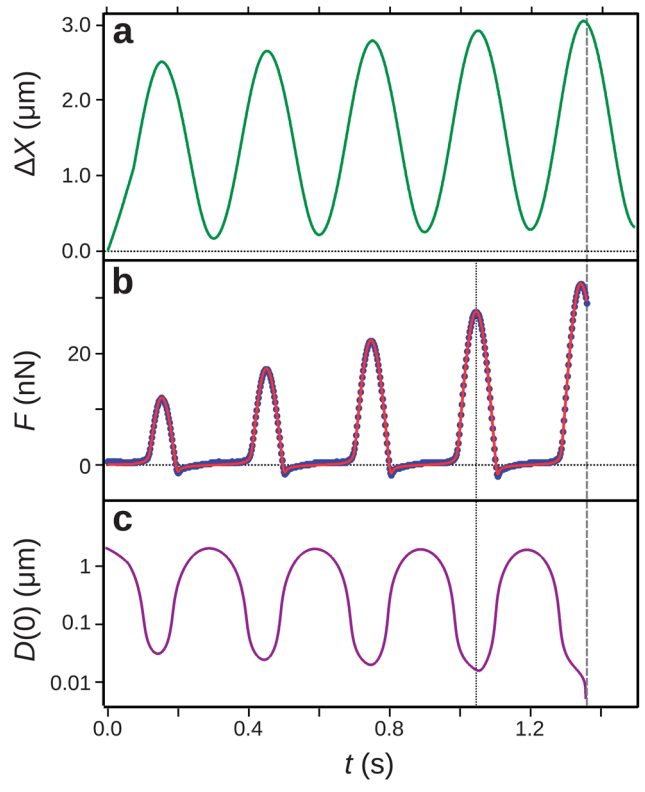

Fig. 2 Two air bubbles, radii 60 and 45 μm, interacting in water at pH 5, where the top bubble is driven with a sinusoidal function. (a) The distance travelled by the cantilever, Δ*X* as a function of time, *t* as measured by the LVDT sensor; (b) the force, *F*, as measured by the AFM cantilever (filled circles – note that every 5th point is displayed for clarity) and the model prediction of the same (solid line) generated as described in the text; (c) evolution of the central film thickness, *D*(0) during the course of the measurement. Minimum film thickness occurs after the force maximum (solid vertical line). In all panels, the vertical dashed line shows the point at which the two bubbles coalesced.

From Fig. 2 it can be seen that as the bubbles are pushed together during each cycle, a repulsive (by convention positive) force is felt between them, representing the hydrodynamic resistance of fluid in the film generated in the presence of a weakly repulsive disjoining pressure. This pressure arises from the overlap of symmetrical electrical double-layers associated with surface charges on the approaching air–water interfaces. It has been posited that these charges arise from strong adsorption of hydroxide ions.[31,32] As the bubbles are pulled apart, the force between then decreases rapidly and becomes negative. This negative force is purely due to the hydrodynamic 'suction' effect, as fluid struggles to re-fill the thinned film between the bubbles. It can be seen from the vertical dotted line in Fig. 2 that the minimum film thickness occurs *after* the force maximum. That is, the thinnest film is achieved not at the force maximum as drops are pushed together, but as they are being pulled apart, due to the suction effect in the film counteracting their separation. If the suction force on retraction can overcome any repulsion between the bubbles then coalescence can occur. In this case, coalescence occurs during a 'retraction' phase of the cycle, suggesting that the hydrodynamic suction is primarily responsible for thinning the film to a critical value.

The bubble coalescence experiment was conducted in water at pH 5, and so the expected surface forces experienced by the bubbles would be a weak electrical double-layer repulsion and a strong van der Waals attraction;[33,34] hence, the overall disjoining pressure can be readily calculated. Using this disjoining pressure and other measured parameters (bubble radii, contact angles and surface tension of 72 ± 1 mN m^{-1}) as an input, the model prediction was obtained. It can be seen from Fig. 2 that there is excellent agreement between theoretical predictions and experimental observations in both the time variation of the force and the moment of bubble coalescence. Significantly, the model also provides the shape of the bubble interfaces at each timestep during the interaction, and so the film shape and separation of the interfaces can be plotted, the latter of which is shown in Fig. 2c. It is clear that on each cycle as the bubbles are

‡ An adaptive correction method using the LVDT to adjust position during the course of the measurement, known as closed-loop control can be used to improve the fidelity with which a supplied functional form is recreated; however, this feedback can introduce noise which may be at unacceptable levels, and was not used here. It is important to note that in modelling the interaction to predict the force, the *experimentally measured* position is used, rather than the (less accurate) assumed position based on drive voltage.

Published on 11 January 2013. Downloaded by The University of Melbourne Libraries on 16/07/2013 07:09:19.

pushed closer together, the film thins more, until at a critical level, the weak electrical double-layer repulsion is overcome by the film suction, and the strong attractive van der Waals force causes the interfaces to coalesce. A visualisation of the modelled force and film profile as a function of time is provided as a video in the ESI.†

It is also important to note that an immobile hydrodynamic boundary condition at the air–water interface is required to reproduce these experimental data using the model. Despite the conventional understanding that pure fluid–fluid interfaces would be expected to demonstrate a mobile condition, corresponding to zero tangential stress at the interface, we have found this not to be the case in this and in previous AFM experiments.[35,36] The coalescence event is extremely rapid and violent, as the interfacial tension acts to minimise the interfacial area of the resulting bubble. Once the film ruptures, no more information can be gained from the AFM data on the mechanism of coalescence. The bubble resulting from coalescence invariably ended up on the cantilever, as the hydrophobised gold patch provided a more energetically favourable contact than the modified silica surface.

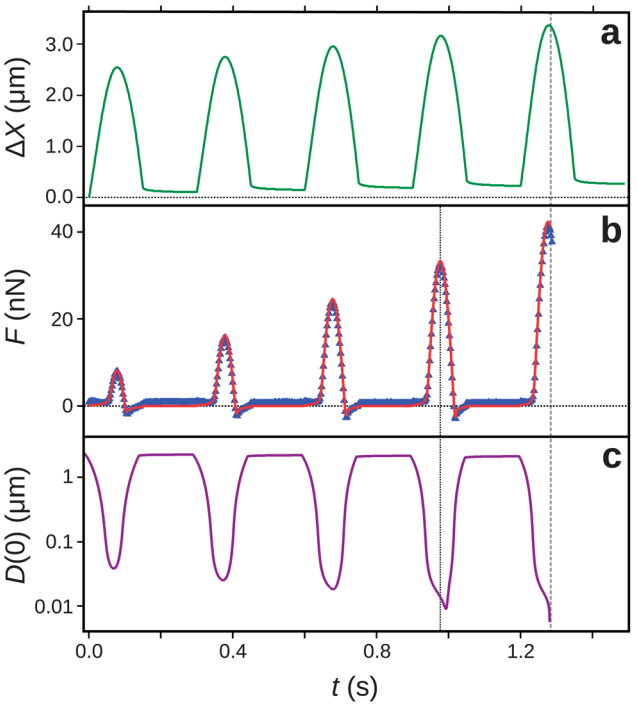

Fig. 3 Interaction between two air bubbles, radii 44 and 51 μm, in water at pH 5, driven with a diaphragm pump-type motion. (a) The distance travelled by the cantilever, ΔX as a function of time, t as measured by the LVDT sensor; (b) the force as measured by the cantilever (symbols) and the model prediction (solid line); (c) the modelled thickness of the liquid film between the two drops at the centre of axisymmetry as a function of time. Minimum film thickness occurs after the force maximum (solid vertical line). In all plots, the vertical dashed line shows the experimental point of coalescence.

Diaphragm and peristaltic pumping

Diaphragm pumping[26] and peristaltic pumping[25] are both ubiquitous in micro-scale systems due to the ease with which they can be implemented mechanically at small scales. However, they generate distinctly different fluid flow characteristics.

The interaction between two bubbles when driven with a characteristic diaphragm pumping drive[26] is shown in Fig. 3. In this instance and for the sinusoidal drive above, the amplitude is increased slightly during each cycle, accompanied by a modest increase in the approach and retract velocity. Both the sinusoidal and diaphragm-type pumping drives show a smooth behaviour at close approach of the bubbles. However, when the bubbles are far apart, the diaphragm pump has a section of zero velocity, where in a real system, the flow would be stopped by a valve. It can be seen that there is in fact little difference in the characteristic force behaviour of the two bubbles between the sinusoidal and diaphragm drive. This is because the hydrodynamics that control lubrication and film behaviour at close approach, and hence are responsible for the forces seen, respond quickly on the timescale of the measurement and so each pumping cycle is effectively decoupled. Here, coalescence is caused due to an increase in the *amplitude* with which the bubbles are driven. The temporal difference between the force maximum and the minimum stable film thickness attained (shown by the dotted line in Fig. 3) is even more pronounced in this case, suggesting a greater influence of hydrodynamic suction in the fourth cycle.

When moving to a peristaltic-type drive function,[25] the behaviour of the two bubbles is quite different (Fig. 4). The key difference between the peristaltic drive and the sinusoidal or diaphragm drives lies in the retract portion of the drive function. The retraction phase of the peristaltic drive commences with a high initial velocity and then decelerates whereas the retraction in the sinusoidal or diaphragm drive begins slowly and accelerates. The result of this characteristic difference is that the suction force felt on retract in a peristaltic drive is maximised at close approach, just as the bubbles begin to separate. This results in a rapid thinning of the film and so the bubbles coalesce on an earlier drive cycle, and coalesce earlier within the cycle itself (Fig. 4).

Analysis of accelerating drives

It has been seen in microfluidics experiments that rapid separation of droplets in close proximity can favour coalescence during droplet interactions. Both Bibette *et al.*[23] and Gunes *et al.*[24] noted that when droplets accelerate away from one another due to the chosen non-linear channel geometry causing an increase in flow rate, coalescence occurred. This elegant demonstration is backed up by previous AFM work using bubbles by Vakarelski *et al.*[12] where it was seen that under certain dynamic conditions, bubbles would coalesce on retract. The reason for this is the hydrodynamic suction force experienced by the bubbles during retraction, which causes a critical thinning of the film between them.

To provide insight into this counter-intuitive situation, we probe coalescence in a cyclic pumping drive scenario *without* increasing the force applied, or decreasing the separation of two drops, but where coalescence could be achieved by *increasing*

 This journal is © The Royal Society of Chemistry 2013

Published on 11 January 2013. Downloaded by The University of Melbourne Libraries on 16/07/2013 07:09:19.

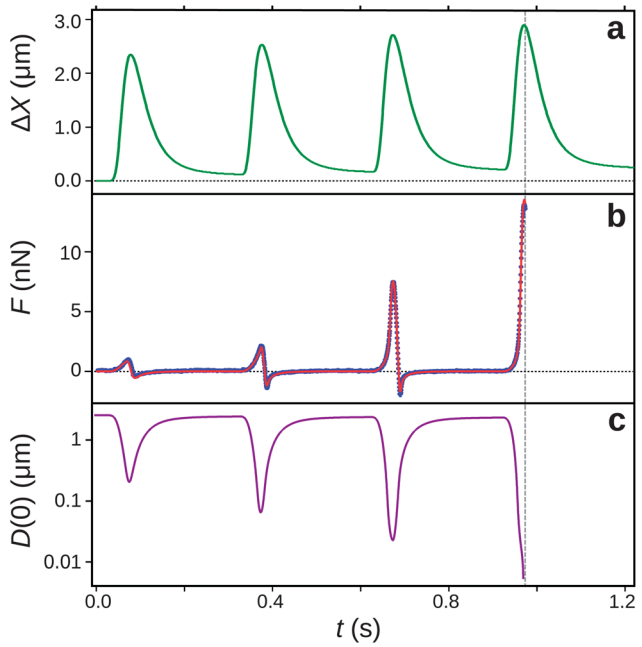

Fig. 4 Interaction between two air bubbles, radii 47 and 39 μm, in water at pH 5, driven with a peristaltic pump-type motion. (a) The distance travelled by the cantilever, ΔX as a function of time, t as measured by the LVDT sensor; (b) the force as measured by the cantilever (symbols) and the model prediction (solid line); (c) the modelled thickness of the liquid film between the two drops at the centre of axisymmetry as a function of time. In all plots, the vertical dashed line shows the experimental point of coalescence.

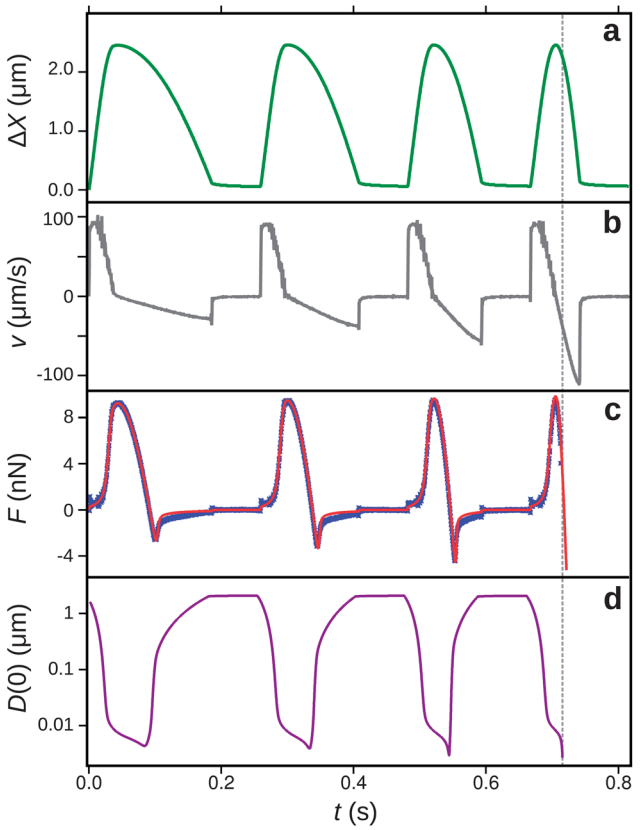

Fig. 5 Interaction between two perfluorooctane droplets, radii 50 and 36 μm, in water at pH 3.2. (a) The distance travelled by the cantilever, ΔX as a function of time, t as measured by the LVDT sensor; (b) the velocity of the piezo (measured) as a function of time; (c) the force as measured by the cantilever (symbols) and the model prediction (solid line); (d) the modelled thickness of the liquid film between the two drops at the centre of axisymmetry as a function of time. In all plots, the vertical dashed line shows the experimental point of coalescence.

the speed at which the drops are pulled apart. That is, a system that appears stable for a given set of conditions can be rendered coalescent by accelerating two drops apart. Thus, we employed a drive function in which the approach trajectory is identical on each cycle with a sine-type function, but with increasing acceleration in successive retraction cycles (Fig. 5).

To demonstrate this effect, a significantly more sensitive system was required than could be provided by air bubbles in water. As the van der Waals force at small separation is so great for two bubbles, thin but stable films could not be achieved with which to test this theory; the velocities required to induce the transition between a metastable and coalescent system are much greater than the $\approx$100 μm s^{-1} available with the AFM. Instead, we consider the coalescence of two perfluorooctane (PFO) drops in water, for which the van der Waals attraction is two orders of magnitude smaller than that between bubbles in water, with a Hamaker constant of $\approx 5 \times 10^{-22}$ J *vs.* $\approx 3.7 \times 10^{-20}$ J. Thus, the surface force acting to cause coalescence is significantly reduced, and a velocity capable of inducing critical film thinning could be easily achieved.

It can be seen in Fig. 5 that by increasing velocity on the retract portion of the drive, coalescence can be induced, and that this is due to a critical thinning of the intervening liquid film between the drops. At low retraction speeds, the film does not thin sufficiently to allow the van der Waals force to take over and cause coalescence. However, once a critical velocity threshold is passed, in this case of around ~50 μm s^{-1}, the hydrodynamic suction is sufficient to overcome the weak double-layer repulsion to an extent that the van der Waals attraction causes a rupturing of the film. It is important to note that the critical velocity required for this transition in behaviour is very system-specific, as the rigidity of the drops from their interfacial tension counteracts the suction force acting on the interface. Hence, this behaviour is not universal, and model predictions are required for each system under scrutiny. A visualisation of the modelled force and film profile as a function of time is provided as a video in the ESI.†

Predictions of stability for selected systems

Thus far we have shown that the model can be used to give insight into experimental measurements, by providing the spatial and temporal properties of the drop or bubble interfaces as they interact. From this, it is possible to determine the relative importance of hydrodynamics and surface forces, and to understand phenomena such as coalescence when droplets are pulled apart.

However, the model can also be used as a powerful predictive tool, and in this capacity it is able to provide guidance on systems *before* any measurements are made. For any system in which the disjoining pressure can be calculated or predicted, the model can

Published on 11 January 2013. Downloaded by The University of Melbourne Libraries on 16/07/2013 07:09:19.

be used to determine the stability and coalescence behaviour of two drops or bubbles over a range of drive conditions, in order to inform channel design or pumping choice for specific purposes. In this format, a small amount of computational effort can be expended to potentially save a great deal of time and physical resources that would otherwise be expended through trial and error. A simple example wherein the model is used predictively is shown in Fig. 6, where the coalescence behaviour of two bubbles driven with a sinusoidal function is determined, using identical parameters to those for the experiment shown in Fig. 2 (except with a surface potential at the air–water interfaces of −72 mV, equivalent to around pH 7.5 for air bubbles).[34,37] The result is a 'map' that points to the conditions where drops are stable or unstable during collisions. In this plot, the amplitude and frequency are simply the parameters of the sine function with which the bubbles are driven. To relate these to 'conventional' AFM parameters, the amplitude refers to the distance which the bubbles are pushed together during the experiment (the force-ramp distance). The frequency is inversely related to the velocity, at constant amplitude, with which approaching and retracting interactions occur.

As the starting separation of the drops was 2 μm, coalescence clearly cannot occur until the amplitude is close to this value. It is seen that at low frequencies, where effective interaction velocities are low, the water film between the bubbles has sufficient time to drain during the approach phase and results in coalescence. However, as the speed increases with increasing frequency at constant amplitude, drainage of the film is incomplete at the maximum force (as for the coalescence event in Fig. 2) but the hydrodynamic suction that occurs as the drops are pulled apart at higher speed thins the film enough to allow the attractive van der Waals interaction to take effect and cause coalescence. However, at much higher retraction speeds, the thin film will have insufficient time to drain during retraction for coalescence to occur. The interesting re-entrant stable behaviour at high frequency and high amplitude follows from the fact that increasing amplitude at constant frequency increases the velocity. A higher velocity on approach will create a larger repulsive hydrodynamic pressure, which results in a thicker film at the point of retraction than that obtained at a lower amplitude with the same drive frequency. As a consequence, the hydrodynamic suction upon retraction from a higher amplitude is not sufficient to thin the film to the point were the attractive van der Waals interaction can take effect to cause coalescence. Taken together, the global behaviour summarised in this figure has clear implications in selecting pumping parameters to drive microfluidic transport.

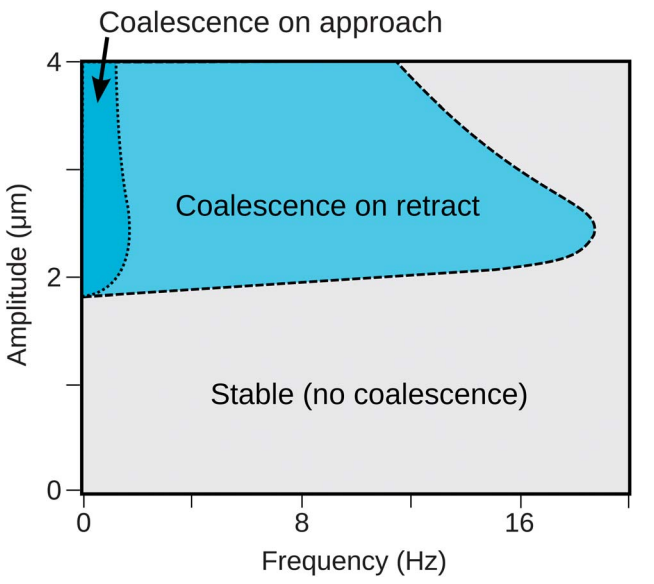

Fig. 6 A predicted stability map or 'phase diagram' for the interaction of two air bubbles in water with radii 60 and 45 μm, and a surface potential of −72 mV. The bubbles are driven with a regular sinusoidal drive function from a starting separation of 2 μm.

The drive functions presented in this work were chosen to demonstrate the capabilities of the AFM as a tool for analysing the types of interactions present in microfluidic devices, and to highlight some interesting behaviours available to droplet systems. However, the principle could be extended to provide a direct analysis of any driven collisions between drops in microfluidic devices and elsewhere. In the scaling shown here, where deformation at close approach is far less than the droplet size, the deviation from sphericity of the drops during interaction is relatively small. Hence, by simply obtaining the droplet position in a microfluidic device (for example by video microscopy and image analysis) it would be relatively facile to mimic collisions using either the AFM or model, or preferably both.

Conclusions

We have demonstrated a new protocol for using the atomic force microscope (AFM) to study collisions between micron-scale drops and bubbles driven with non-linear velocities. By emulating the droplet trajectories expected for flows driven by simple pumping drives, information on the physical parameters and conditions required for coalescence to occur were obtained. It is seen that, in line with expectation for dynamic collisions in metastable systems, coalescence may be favoured when the drops are accelerating away from one another, due to the hydrodynamic suction force thinning the film of liquid between them and causing rupture. Using a model which accounts for deformation of drops, surface forces and hydrodynamic lubrication we are able to model extant experimental data for droplet collisions, and also to predict the behaviour of as yet unexplored systems, providing a tool to aid in the design of future fluid handling devices by providing a 'stability map' for droplet interactions. Significantly, this protocol can easily be extended to understanding the behaviour of 'free' drops and bubbles interacting, which inevitable occurs *via* non-linear drop velocities. Further challenges emerge, such as the analysis of non-axisyemmtric (off-centre) collisions, which is vital to understanding the interactions of free drops in micro-scale systems; work into this problem is ongoing.

Acknowledgements

This project is funded in part by the Australian Research Council through a Discovery Project Grant. C.W. is supported by

 This journal is © The Royal Society of Chemistry 2013

Published on 11 January 2013. Downloaded by The University of Melbourne Libraries on 16/07/2013 07:09:19.

an Australian Postgraduate Research Award. The PFPC is thanked for infrastructure support.

References

1 C. Baroud, F. Gallaire and R. Dangla, *Lab Chip*, 2010, **10**, 2032–2045.
2 B. J. Adzima and S. S. Velankar, *J. Micromech. Microeng.*, 2006, **16**, 1504–1510.
3 J. J. Agresti, E. Antipov, A. R. Abate, K. Ahn, A. C. Rowat, J.-C. Baret, M. Marquez, A. M. Klibanov, A. D. Griffiths and D. A. Weitz, *Proc. Natl. Acad. Sci. U. S. A.*, 2010, **107**, 4004–4009.
4 P. S. Dittrich and A. Manz, *Nat. Rev. Drug Discovery*, 2006, **5**, 210–218.
5 Y. Chen, T.-H. Wu and P.-Y. Chiou, *Lab Chip*, 2012, **12**, 1771–1774.
6 A. Sin, C. F. Reardon and M. L. Shuler, *Biotechnol. Bioeng.*, 2004, **85**, 359–363.
7 P. Skafte-Pedersen, D. Sabourin, M. Dufva and D. Snakenborg, *Lab Chip*, 2009, **9**, 3003–3006.
8 M. Pascaline, A. R. Abate, J. J. Agresti and D. A. Weitz, *Biomicrofluidics*, 2011, **5**, 024101.
9 N. Bremond and J. Bibette, *Soft Matter*, 2012, **8**, 10549–10559.
10 R. F. Tabor, F. Grieser, R. R. Dagastine and D. Y. C. Chan, *J. Colloid Interface Sci.*, 2012, **371**, 1–14.
11 H.-J. Butt, R. Berger, E. Bonnacurso, Y. Chen and J. Wang, *Adv. Colloid Interface Sci.*, 2007, **133**, 91–104.
12 I. U. Vakarelski, R. Manica, X. Tang, S. J. O'Shea, G. W. Stevens, F. Grieser, R. R. Dagastine and D. Y. C. Chan, *Proc. Natl. Acad. Sci. U. S. A.*, 2010, **107**, 11177–11182.
13 R. R. Dagastine, R. Manica, S. L. Carnie, D. Y. C. Chan, G. W. Stevens and F. Grieser, *Science*, 2006, **313**, 210–213.
14 D. Y. C. Chan, R. R. Dagastine and L. R. White, *J. Colloid Interface Sci.*, 2001, **236**, 141–154.
15 D. Y. C. Chan, R. Manica and E. Klaseboer, *Soft Matter*, 2011, **7**, 2235–2264.
16 D. Y. C. Chan, E. Klaseboer and R. Manica, *Adv. Colloid Interface Sci.*, 2011, **165**, 70–90.
17 R. Manica, J. N. Connor, R. R. Dagastine, S. L. Carnie, R. G. Horn and D. Y. C. Chan, *Phys. Fluids*, 2008, **20**, 032101/1–032101/12.
18 A. Gromer, R. Penfold, A. P. Gunning, A. R. Kirby and V. J. Morris, *Soft Matter*, 2010, **6**, 3957–3969.
19 R. F. Tabor, R. Manica, D. Y. C. Chan, F. Grieser and R. R. Dagastine, *Phys. Rev. Lett.*, 2011, **106**, 064501/1–064501/4.
20 R. F. Tabor, C. Wu, H. Lockie, R. Manica, D. Y. C. Chan, F. Grieser and R. R. Dagastine, *Soft Matter*, 2011, **7**, 8977–8983.
21 L. R. Fisher, D. Hewitt, E. E. Mitchell, J. Ralston and J. Wolfe, *Adv. Colloid Interface Sci.*, 1992, **39**, 397–416.
22 M. H. W. Hendrix, R. Manica, E. Klaseboer, D. Y. C. Chan and C.-D. Ohl, *Phys. Rev. Lett.*, 2012, **108**, 247803.
23 N. Bremond, A. R. Thiam and J. Bibette, *Phys. Rev. Lett.*, 2008, **100**, 024501/1–024501/4.
24 Z. D. Gunes, X. Clain, O. Breton, G. Mayor and A. Burbidge, *J. Colloid Interface Sci.*, 2010, **343**, 79–86.
25 P. Hariharan, V. Seshadri and R. K. Banerjee, *Math. Comput. Model.*, 2008, **48**, 998–1017.
26 M. T. Taylor, P. Nguyen, J. Ching and K. E. Petersen, *J. Micromech. Microeng.*, 2003, **13**, 201–208.
27 J. L. Hutter and J. Bechhoefer, *Rev. Sci. Instrum.*, 1993, **64**, 1868–1873.
28 I. U. Vakarelski, J. Lee, R. R. Dagastine, D. Y. C. Chan, G. W. Stevens and F. Grieser, *Langmuir*, 2008, **24**, 603–605.
29 S. Biggs and F. Grieser, *J. Colloid Interface Sci.*, 1994, **165**, 425–430.
30 R. F. Tabor, H. Lockie, D. Mair, R. Manica, D. Y. C. Chan, F. Grieser and R. R. Dagastine, *J. Phys. Chem. Lett.*, 2011, **2**, 961–965.
31 J. K. Beattie and A. M. Djerdjev, *Angew. Chem., Int. Ed.*, 2004, **43**, 3368–3571.
32 P. Creux, J. Lachaise, A. Graciaa, J. K. Beattie and A. Djerdjev, *J. Phys. Chem. B*, 2009, **113**, 14146–14150.
33 J. N. Israelachvili, *Intermolecular and Surface Forces*, Academic Press, San Diego, 1991.
34 R. F. Tabor, D. Y. C. Chan, F. Grieser and R. R. Dagastine, *Angew. Chem., Int. Ed.*, 2011, **50**, 3454–3456.
35 R. R. Dagastine, G. B. Webber, R. Manica, G. W. Stevens, F. Grieser and D. Y. C. Chan, *Langmuir*, 2010, **26**, 11921–11927.
36 H. Lockie, S. McLean and R. R. Dagastine, *J. Phys. Chem. Lett.*, 2011, **2**, 2472–2477.
37 M. Takahashi, *J. Phys. Chem. B*, 2005, **109**, 21858–21864.